Pressurizing Field-Effect Transistors of Few-Layer MoS₂ in a Diamond Anvil Cell

Yabin Chen,[†] Feng Ke,[‡] Penghong Ci,[†] Changhyun Ko,[†] Taegyun Park,[†] Sahar Saremi,[†] Huili Liu,[†,§] Yeonbae Lee,[§] Joonki Suh,[†] Lane W. Martin,[†] Joel W. Ager,[†,§] Bin Chen,[‡] and Junqiao Wu*[†,§]

[†]Department of Materials Science and Engineering, University of California, Berkeley, California 94720, United States
[‡]Center for High Pressure Science and Technology Advanced Research, Shanghai 201203, China
[§]Materials Sciences Division, Lawrence Berkeley National Laboratory, Berkeley, California 94720, United States

S *Supporting Information*

ABSTRACT: Hydrostatic pressure applied using diamond anvil cells (DAC) has been widely explored to modulate physical properties of materials by tuning their lattice degree of freedom. Independently, electrical field is able to tune the electronic degree of freedom of functional materials via, for example, the field-effect transistor (FET) configuration. Combining these two orthogonal approaches would allow discovery of new physical properties and phases going beyond the known phase space. Such experiments are, however, technically challenging and have not been demonstrated. Herein, we report a feasible strategy to prepare and measure FETs in a DAC by lithographically patterning the nanodevices onto the diamond culet. Multiple-terminal FETs were fabricated in the DAC using few-layer MoS₂ and BN as the channel semiconductor and dielectric layer, respectively. It is found that the mobility, conductance, carrier concentration, and contact conductance of MoS₂ can all be significantly enhanced with pressure. We expect that the approach could enable unprecedented ways to explore new phases and properties of materials under coupled mechano-electrostatic modulation.

KEYWORDS: *Hydrostatic pressure, diamond anvil cell, MoS₂, h-BN dielectric, field-effect transistor*
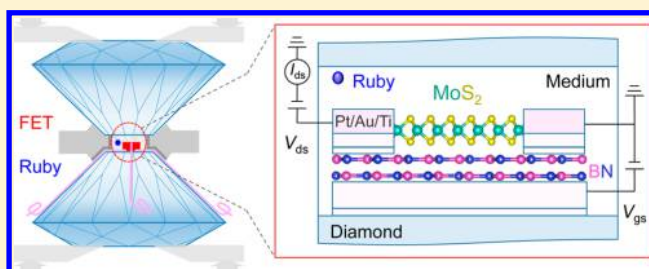
The key reason that semiconductors are extensively used in various device applications is that their physical properties can be conveniently tuned by external stimuli, such as electrical or optical fields, temperature, and stress/pressure.[1−6] By injecting excess charge carriers with electrostatic fields, electrical conductivity of a typical semiconductor could be dramatically modulated, and this effect lays the foundation for operation of the basic device unit of information technology, the field-effect transistor (FET). Electrostatic fields can also influence many other physical properties of materials. For example, doped molybdenum disulfide (MoS₂), as a representative two-dimensional (2D) transition metal dichalcogenide, undergoes a sequence of semiconducting-metallic-superconducting phase transitions at high fields;[7,8] and layered TaS₂ exhibits layer-dependent charge density waves that are also field-dependent.[9] On the other hand, high hydrostatic pressure, i.e., isotropic pressure applied to a solid specimen via liquid or amorphous media using a diamond anvil cell (DAC), has been widely utilized to mechanically tune lattice parameters of solid materials, hence modulating their various order parameters, electronic structures, and interfacial coupling.[10−12] The hydrostatic pressure approach has the advantages of being nonintrusive, reversible, "clean" from contamination (unlike chemical doping), and able to impose high strain without cracking the sample (unlike uniaxial stress). For example, MoS₂

displays an isostructural transition from $2H_c$ to $2H_a$ at a pressure of ∼20 GPa,[13,14] and further, becomes a superconductor at 90 GPa with a transition temperature onset of 11.5 K.[15] However, the two modulations with electrical fields and hydrostatic pressure have been, thus far, totally separate; namely, existing experiments probe material response by either varying electrical fields at ambient pressure or varying pressure at zero gating electrical field. Simultaneous application and tuning of pressure and fields onto a solid material have not been demonstrated. In this work, we report for the first time the simultaneous mechano-electrostatic tuning by investigating the behavior of few-layer MoS₂ FET nanodevices inside a DAC. It is found that the electrical performance (i.e., carrier concentration, mobility, and contact quality) of the MoS₂ FETs can be significantly modulated with hydrostatic pressure. We expect that the strategy of fabricating FETs inside the DAC could pave the way to discovering and probing novel properties of solid materials.

Although plenty of electrical conductance measurements in a DAC have been demonstrated on bulk materials,[16−19] the fabrication and measurements of FET nanodevices inside a
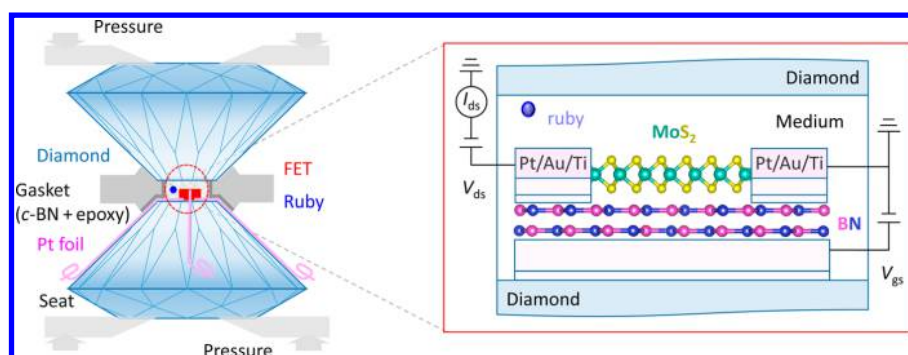
Figure 1. FET nanodevice in a DAC. In this schematic, the layered MoS_2 and h-BN were used as the channel semiconductor and dielectric material, respectively. Each of the electrodes is composed of two parts, a patterned and deposited thin metal line (Au/Ti) inside the DAC chamber connected to a strip of Pt foil outside the chamber. The pressure was calibrated by ruby particles.
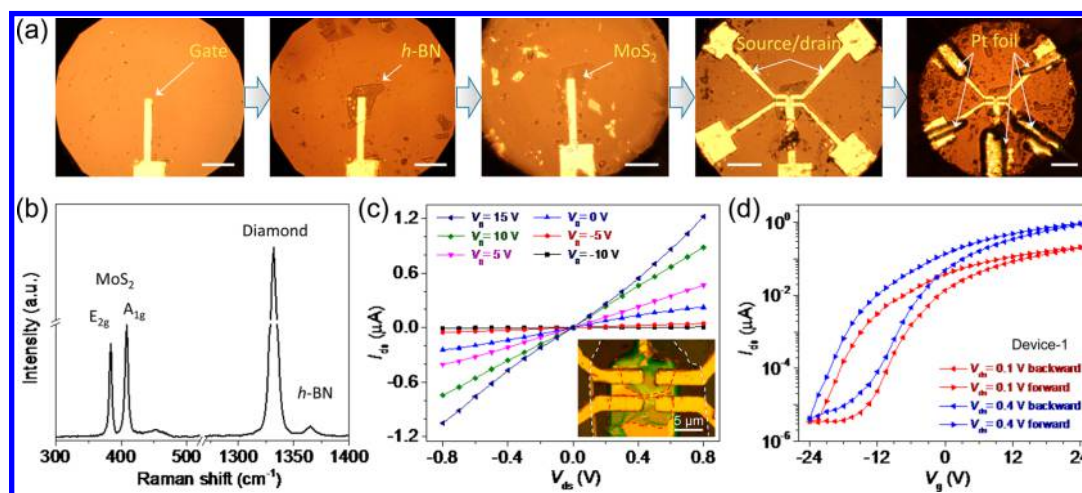

Figure 2. FET of a few-layer MoS_2 on the diamond surface. (a) Fabrication process of a five-terminal MoS_2−FET on the diamond surface. The culet size is 300 μm. The scale bars are 50 μm. (b) Raman spectra of the transferred MoS_2 and h-BN flakes overlapped on the diamond surface. (c) Output curves of the MoS_2−FET nanodevice at ambient pressure. The gate voltage varies from −10 to 15 V. Inset is an optical image of the final device. The red and white dashed lines show the boundary of the MoS_2 and h-BN flakes, respectively. The 3.0 nm-thick MoS_2 flake in this device broke into two discontinued pieces during the exfoliation. (d) Transfer curves of the MoS_2−FET nanodevice under different source-drain voltages.

DAC are still lacking. This lack of studies is due to several immense technical challenges, particularly: 1. Electrical connection between the nanoscale semiconductor channel (e.g., 2D semiconductors) and metal electrodes inside the DAC. Making such connections reliably and stably conductive under high pressure is already notoriously challenging for bulk materials. It becomes even more difficult for 2D materials owing to their intrinsically poor electrical contact with most metals, as well as the fact that the popularly used metal foil (Au or Pt) or silver paste can hardly be applied to the 2D flakes that have a very limited lateral size.[16] 2. Reliability of the dielectric layer. The routinely used, deposited Al_2O_3 or HfO_2 films can easily fracture under high pressure, resulting in considerable leakage currents. 3. Unlike bulk crystals or deposited thin films, it is difficult to transfer 2D flakes onto the desired microscale area on the diamond surface without degrading its crystal structure and physical properties.

To achieve the operation of FET nanodevices under high pressure, we developed a strategy to directly fabricate multiple electrodes onto a 2D semiconductor flake and a layered dielectric inside the tiny DAC chamber. The multiple-electrode system is constituted of metal lines patterned by lithography and deposition onto the diamond surface (Supporting Information, Figure S1), which are connected to strips of Pt

foil leading outside the chamber. We used hexagonal-boron nitride (h-BN) as the dielectric material due to its high breakdown field as well as layered structure that allows for good thickness control and compatibility with high pressure. Figure 1 depicts the configuration of a bottom-gated FET device in DAC. Briefly, cubic-BN (c-BN) was utilized as the coating to the steel gaskets to ensure electrical isolation between different electrodes.[20] Inside the gasket chamber, a strip of Au/Ti layer (50/5 nm) was first deposited as the gate electrode onto the diamond culet following photolithography patterning. The dielectric h-BN and channel semiconductor (few-layer MoS_2 in this work) were sequentially transferred onto the gate electrode. Afterward, four more electrodes were further patterned and deposited onto the four corners of the MoS_2 flake for channel conductance and filed-effect measurements. Finally, each of these patterned electrodes was connected to a narrow strip of Pt foil (~5 μm thick), which was ultimately connected to the external electronics. Importantly, the Pt strips are required to extend into the pressure chamber across the diamond culet edge because the patterned electrodes can rarely survive under high pressures once the gasket is sealed over the diamonds. After careful and optimal alignments, such nanodevices are robust and reproducible enough when the pressure exceeds ~50 GPa (= 500,000 atm), which is sufficiently high to
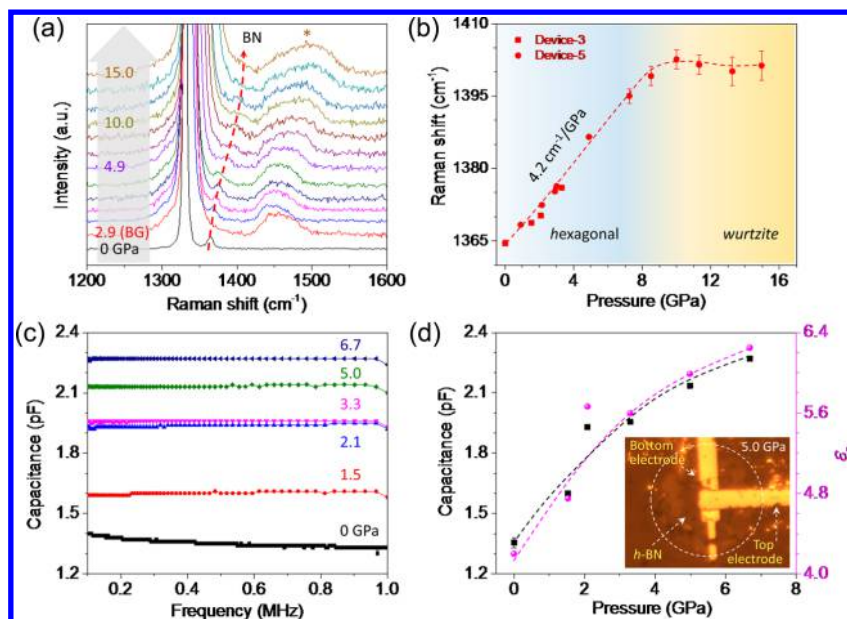
Figure 3. Pressure behavior of the dielectric layer, h-BN. (a) Raman spectrum of a 47 nm-thick h-BN under pressure. The red curve of 2.9 GPa was taken on the blank diamond surface as the background. The black curve of 0 GPa was taken before clamping the cell. The asterisk indicates a broad band arising from the pressure medium. (b) Pressure-dependent Raman shift of h-BN. The change in slope at ~9 GPa signifies a phase transition from hexagonal to wurtzite structure. The circle and square symbols represent two different h-BN flakes. (c) Capacitance measurements of h-BN in the DAC at different pressures. (d) Pressure-dependent capacitance and relative dielectric constant of h-BN. Inset is a typical h-BN device for the capacitance measurements imaged at 5.0 GPa, showing the bottom and top electrodes.

drive structural transitions of most crystalline materials. The device fabrication yields a high success rate of ~80%.

Following this method, few-layer MoS$_2$ FETs were successfully fabricated and measured. An actual process was recorded and shown in Figure 2a. The thickness of the transferred h-BN and MoS$_2$ flakes were ~91 and 3.0 nm, respectively, as confirmed by atomic force microscopy (AFM). It is noted that the gate electrode needs to be well positioned at the center of the pressure chamber, and the lateral size of the active region of the FET (namely, the channel and the gate materials) should be well within the radius of the gasket hole; otherwise, the possible shrinkage of the gasket hole under high pressure may destroy the device. The Pt foil strips were manually aligned with the patterned electrodes under an optical microscope. Raman measurements were carried out on the overlapped MoS$_2$/h-BN region to confirm the successful transfer. As shown in Figure 2b, the four Raman peaks at 383.8, 408.1, 1331.8, and 1365.1 cm^{-1} are consistent with the Raman modes of in-plane E_{2g} of MoS$_2$, out-of-plane A_{1g} of MoS$_2$, first-order F_{2g} of diamond, and first-order E_{2g} of h-BN, respectively (Supporting Information, Figure S2−S3).[21,22] Figure 2c displays the obtained output characteristics between a pair of source-drain electrodes under various gate voltages (the other pair showed similar results). The channel current becomes significantly higher as the gate voltage increases toward positive values, consistent with the expected n-type property of exfoliated MoS$_2$.[23] The nearly linear I−V curves indicate reasonably good contact between the MoS$_2$ and the electrodes. Additionally, the transfer curves in Figure 2d prove excellent dielectric insulation of the h-BN flake. The current on/off ratio, I_{on}/I_{off}, is higher than 10^5. The field effect mobility was extracted from the linear region of the conductance curves. The mobility for this device is ~4 cm^2 V^{-1} s^{-1} calculated using the equation $\mu = [dI_{ds}/dV_g] \times [L/(C_iWV_{ds})]$, where L and W are the channel length and width, respectively, and C_i is the

capacitance per unit area between the channel and the gate electrode.[24] This mobility value is underestimated due to the non-negligible contact resistance. In a latter section, we will eliminate the effect of the contact resistance using four-probe van der Pauw method. The hysteresis in Figure 2d between forward and backward measurements may be attributed to unintentional doping effects from ambient water or oxygen, as reported before.[25] All of these results validate our method of device fabrication and measurements on the diamond culet.

As the dielectric property of the h-BN may vary with pressure, its pressure behavior must be calibrated before we use it to analyze the FET data. We hence investigated the dielectric constant of h-BN under high pressure. Figure 3a shows the Raman spectrum of h-BN in the DAC up to a pressure of 15 GPa. The Raman peak of both h-BN and diamond exhibits a clear blue shift due to the pressure-induced lattice stiffening. By comparison to the background signal, the board band at ~1450 cm^{-1} comes from the pressure medium. As shown in Figure 3b, the Raman shift of h-BN first increases monotonically and then becomes flat, implying a phase transition from the hexagonal phase to the wurtzite phase. The stiffening rate of the hexagonal phase Raman is 4.2 cm^{-1}/GPa, which is in agreement with the literature.[22] More importantly, we carried out capacitance measurements of the h-BN layer in the DAC in order to determine its change in dielectric constant under high pressure, as shown in Figure 3c,d. The extracted capacitance increases monotonically from 1.3 pF at 0 GPa to 2.3 pF at 6.7 GPa. Its relative dielectric constant was calculated using the expression $C = AC_i = A(\varepsilon_0\varepsilon_r/t)$, where A is the overlap area between the h-BN flake and electrodes, ε_r and t are the relative dielectric constant and layer thickness, respectively, and $\varepsilon_0 = 8.85 \times 10^{-12}$ F m^{-1} is the vacuum dielectric constant.[26] The reduction in thickness of h-BN as a function of pressure was calculated using the existing data reported based on X-ray diffraction.[27] The obtained ε_r becomes 1.5 times higher at 6.7 GPa than that at
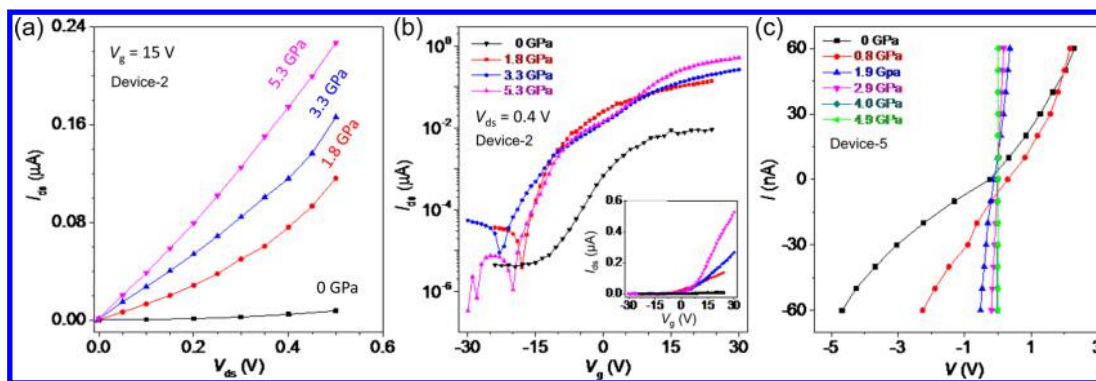
Figure 4. Transport measurements of a MoS$_2$ FET in the DAC. (a) Output curves of a bilayer-MoS$_2$ FET under different pressures. (b) Transfer curves of the same bilayer-MoS$_2$ FET under different pressures. Inset is the same data shown in linear scale. (c) Four-probe I–V curves of a MoS$_2$ FET obtained through the van der Pauw method in the DAC, where the MoS$_2$ flake is 3−5 layers.
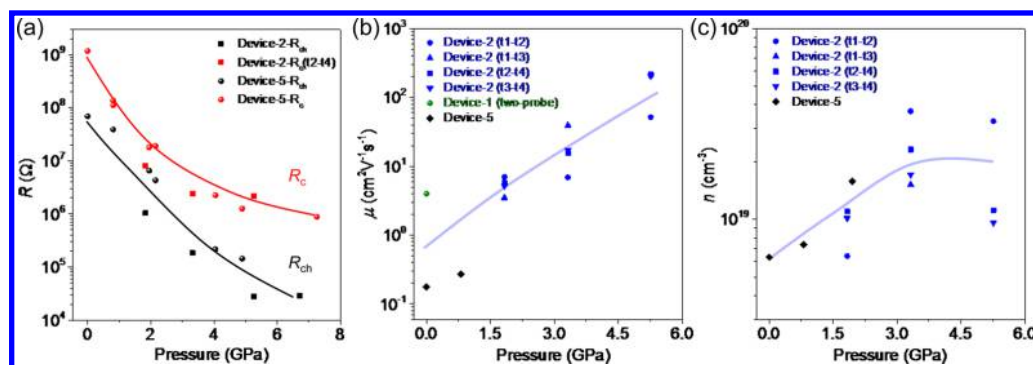

Figure 5. (a) Channel resistance (black) and contact resistance (red) of MoS$_2$−FET devices as a function of pressure. (b) Pressure-dependent mobility of MoS$_2$ flakes in the DAC. The t1 to t4 indicate the electrode number from the same FET nanodevice (further details in Supporting Information, Figure S4). (c) Extracted carrier concentration of MoS$_2$ flakes as a function of pressure. The MoS$_2$ flakes are bilayer and 3−5 layers in device 2 and 5, respectively. All lines are drawn to guide the eye.

ambient pressure, an effect that can be explained by the pressure-induced bandgap (E_g) reduction of h-BN[28] following the empirical Moss relation, $\varepsilon_r^2 E_g \approx 95$ eV for most semiconductors.[29] As its bandgap becomes smaller, h-BN has a higher ε_r and can more effectively screen the gating fields for the channel MoS$_2$.

Pressure-modulated transport characteristics of MoS$_2$ FETs were investigated, and a typical one is shown in Figure 4. For a given V_g, the source-drain current I_{ds} increases dramatically as the pressure increases, which is in agreement with the expected pressure-induced reduction in bandgap and resistance of MoS$_2$.[13] Figure 4b displays the pressure-dependent transfer characteristics of a MoS$_2$ FET. The on-state current clearly increases as the pressure increases from 0 to 5.3 GPa. We further measured the real channel resistance, R_{ch}, using the four-probe van der Pauw method on the MoS$_2$ flake. In this method, a constant current of 100 nA was flowed between two adjacent electrodes, and the other, opposite pair of electrodes probed the voltage drop. As seen from Figure 4c, the MoS$_2$ channel becomes monotonically more conductive as pressure increases. The I–V curve also becomes more linear at higher pressures, indicating that the pressure improves the electrical contact. The decreased R_{ch} contributed significantly to the improved two-probe conductance in Figure 4a,b.

Next, we separate the contact resistance R_c from the channel resistance R_{ch} using the four-probe data in Figure 4c via $R_{tot} = R_{ch} + 2R_c$, where R_{tot} is the obtained two-probe total resistance. R_{ch} is extracted by the van der Pauw method (more details in

Supporting Information). The resultant data is plotted in Figure 5a and shows two effects: 1. the contact resistance R_c drops drastically with pressure, and more importantly, 2. the channel resistance R_{ch} also decreases rapidly with pressure. The improved contact quality is expected from the reduced Schottky barrier at the contact. The Schottky barrier height between n-type MoS$_2$ and Ti metal is reported to be ∼50 meV, after a pinning of the Ti Fermi level near the conduction band of MoS$_2$ (the work function of Ti is ∼4.3 eV, and electron affinity of MoS$_2$ is ∼4.0 eV).[30] Theoretical calculations predict that hydrostatic pressure rapidly pushes down the conduction band minimum of few-layer MoS$_2$ toward a better alignment with the Fermi level of Ti.[31] As a result, the Schottky barrier height between the Ti and MoS$_2$ is reduced, resulting in a lower contact resistance. The high pressure may also mechanically push the electrode against the MoS$_2$ flake, effectively enlarging the contact area at the microscale, which contributes to lowering the contact resistance.

We note that the contact resistance R_c is very high in our case. Normally a thermal annealing (∼300 °C) is typically used to improve the evaporated contact on such transition metal dichalcogenides, while the annealing was not used here because it is incompatible with our diamond anvil cell experiments because the glue used to mount the diamond does not survive that high temperature. Ideally, the van der Pauw method requires Ohmic contacts between the MoS$_2$ flake and the four deposited electrodes. The nonlinear I–V behavior at low pressures (Figure 4c) indicates existence of Schottky barriers,

which may cause underestimation of the channel conductivity and mobility. Since the contact quality was improved as pressure increases, the trend of improved device performance with pressure (Figure 5) and the explanation are at least qualitatively accurate.

Following the analysis, we subsequently calculated the pressure dependence of the field-effect mobility μ and electron concentration n of MoS_2, as shown in Figure 5b,c. The mobility was extracted from the transfer curves in Figure 4b using $\mu = [dI_{ds}/dV_g] \times [L/(C_i WV_{ds(ch)})]$, where $V_{ds(ch)}$ is the calibrated voltage drop solely onto the channel that eliminates the effects of contact resistance (more details in Supporting Information). The obtained mobility shows a significant improvement with pressure. This improvement can be, at least partially, attributed to the reduced electron effective mass m^* under pressure that has been predicted by *ab initio* calculations.[32] According to the Drude model, μ is inversely proportional to m^* as $\mu = e\tau/m^*$. Assuming that the relaxation time τ is less sensitive to external pressure (because pressure does not severely alter the electron-scattering centers in the channel such as impurity and surface condition of MoS_2), an improved μ is expected. Finally, the carrier concentration n increases following $n = 1/(e\mu\rho_{ch})$, where ρ_{ch} is the channel resistivity. This is consistent with the reduction in m^* and in bandgap of MoS_2 under high pressure.[32] Generally, the unintentionally doped free electrons in exfoliated MoS_2 flakes originate from native defects such as sulfur vacancies. These native defects act as shallow donors and donate free electrons to the conduction bands of MoS_2 upon thermal excitation at room temperature. According to the hydrogen defects model, the ionization energy of these shallow donors is 13.6 eV $\times m^*/\varepsilon_r^2$, where ε_r is the relative dielectric constant of MoS_2, which is expected to also follow the empirical Moss relation with its bandgap as discussed earlier for h-BN. The pressure driven reduction in both m^* and bandgap of MoS_2 thus reduces the ionization energy of these shallow donors, resulting in an increase in free electron density. The degenerately high free electron density might also more strongly screen some of the carrier scattering centers, which helps to increase the electron mobility.

In conclusion, we report the behavior of few-layer MoS_2 flakes under both hydrostatic pressure and gating fields by assembling them into the FET configuration inside a DAC. For the first time, our technique enables simultaneous, *in situ* electronic and structural modulation of the channel material by electrostatic and pressure means. It is found that the carrier mobility and density in the channel, as well as the contact conductance, can all be remarkably improved with the hydrostatic pressure. We believe that our methodology can be widely employed for unprecedented exploration of condensed matter under simultaneous tuning with electrical fields (electrostatic gating) and mechanical (pressure) forces.

Methods. *Device Preparation and Characterization.* The MoS_2 and h-BN flakes were mechanically exfoliated onto a Si substrate (300 nm oxide layer). They were sequentially transferred onto the gate electrode by a polydimethylsiloxane transfer method.[12] The flake thickness was confirmed by tapping-mode scanning of AFM (Nanoscope 3D). The micro-Raman measurements were carried out using the commercial Renishaw Raman spectroscope, and the laser wavelength was 488 nm. All devices were prepared by following the standard photolithography and lift-off process. The Ti/Au films as the inner electrodes were deposited by electron beam evaporation in a chamber with pressure lower than 10^{-7} Torr. The

capacitance of the h-BN devices was measured by a LCR meter (Aligent E4980A).

High Pressure Measurement in the DAC. Hydrostatic pressure was generated by a symmetric DAC with 300 μm culet size (type IA diamond). A mixture of c-BN powder and epoxy was used as the insulating coating for the steel gaskets. The fabrication method has been reported elsewhere.[20] The preindented thickness of gasket was within 40 μm, and a hole of 100 μm drilled by laser was utilized as the pressure chamber. Daphne 7373[33] was used as the pressure-transmitting medium. The thickness of the Pt foil was around 5 μm, and it was manually cut by a sharp blade into narrow strips (<10 μm) as the outer electrodes. The pressure was calibrated by the photoluminescence of ruby particles placed next to the sample inside the pressure chamber.[34]

ASSOCIATED CONTENT

Supporting Information

The Supporting Information is available free of charge on the ACS Publications website at DOI: 10.1021/acs.nano-lett.6b03785.

> R_c and μ extraction with the van der Pauw method; negligible effects of Daphne 7373 on the properties of MoS_2; additional figures (PDF)

AUTHOR INFORMATION

Corresponding Author
*E-mail: wuj@berkeley.edu.

ORCID
Taegyun Park: 0000-0002-1138-8747
Junqiao Wu: 0000-0002-1498-0148

Author Contributions
Y.C. and F.K. contributed equally to this work.

Notes
The authors declare no competing financial interest.

REFERENCES

(1) Wang, H. T.; Yuan, H. T.; Hong, S. S.; Li, Y. B.; Cui, Y. Physical and chemical tuning of two-dimensional transition metal dichalcogenides. *Chem. Soc. Rev.* **2015**, *44* (9), 2664−2680.

(2) Li, L. K.; Yu, Y. J.; Ye, G. J.; Ge, Q. Q.; Ou, X. D.; Wu, H.; Feng, D. L.; Chen, X. H.; Zhang, Y. B. Black phosphorus field-effect transistors. *Nat. Nanotechnol.* **2014**, *9* (5), 372−377.

(3) Chen, Y. B.; Zhang, S.; Gao, W. W.; Ke, F.; Yan, J. Y.; Saha, B.; Ko, C. H.; Suh, J.; Chen, B.; Ager, J. W.; et al. Pressure-induced

structural transition of $Cd_xZn_{1-x}O$ alloys. *Appl. Phys. Lett.* **2016**, *108* (15), 152105−152108.

(4) Ye, Y.; Wong, Z. J.; Lu, X. F.; Ni, X. J.; Zhu, H. Y.; Chen, X. H.; Wang, Y.; Zhang, X. Monolayer excitonic laser. *Nat. Photonics* **2015**, *9* (11), 733−737.

(5) Conley, H. J.; Wang, B.; Ziegler, J. I.; Haglund, R. F.; Pantelides, S. T.; Bolotin, K. I. Bandgap engineering of strained monolayer and bilayer MoS_2. *Nano Lett.* **2013**, *13* (8), 3626−3630.

(6) Mak, K. F.; Shan, J. Photonics and optoelectronics of 2D semiconductor transition metal dichalcogenides. *Nat. Photonics* **2016**, *10* (4), 216−226.

(7) Costanzo, D.; Jo, S.; Berger, H.; Morpurgo, A. F. Gate-induced superconductivity in atomically thin MoS_2 crystals. *Nat. Nanotechnol.* **2016**, *11* (4), 339−344.

(8) Biscaras, J.; Chen, Z. S.; Paradisi, A.; Shukla, A. Onset of two-dimensional superconductivity in space charge doped few-layer molybdenum disulfide. *Nat. Commun.* **2015**, *6*, 8826.

(9) Yu, Y. J.; Yang, F. Y.; Lu, X. F.; Yan, Y. J.; Cho, Y. H.; Ma, L. G.; Niu, X. H.; Kim, S.; Son, Y. W.; Feng, D. L.; et al. Gate-tunable phase transitions in thin flakes of 1T-TaS_2. *Nat. Nanotechnol.* **2015**, *10* (3), 270−276.

(10) Drozdov, A. P.; Eremets, M. I.; Troyan, I. A.; Ksenofontov, V.; Shylin, S. I. Conventional superconductivity at 203 K at high pressures in the sulfur hydride system. *Nature* **2015**, *525* (7567), 73−77.

(11) Dalladay-Simpson, P.; Howie, R. T.; Gregoryanz, E. Evidence for a new phase of dense hydrogen above 325 gigapascals. *Nature* **2016**, *529* (7584), 63−67.

(12) Fan, W.; Zhu, X.; Ke, F.; Chen, Y. B.; Dong, K. C.; Ji, J.; Chen, B.; Tongay, S.; Ager, J. W.; Liu, K.; et al. Vibrational spectrum renormalization by enforced coupling across the van der Waals gap between MoS_2 and WS_2 monolayers. *Phys. Rev. B: Condens. Matter Mater. Phys.* **2015**, *92* (24), 241408.

(13) Nayak, A. P.; Bhattacharyya, S.; Zhu, J.; Liu, J.; Wu, X.; Pandey, T.; Jin, C. Q.; Singh, A. K.; Akinwande, D.; Lin, J. F. Pressure-induced semiconducting to metallic transition in multilayered molybdenum disulphide. *Nat. Commun.* **2014**, *5*, 3731−3739.

(14) Chi, Z. H.; Zhao, X. M.; Zhang, H.; Goncharov, A. F.; Lobanov, S. S.; Kagayama, T.; Sakata, M.; Chen, X. J. Pressure-induced metallization of molybdenum disulfide. *Phys. Rev. Lett.* **2014**, *113* (3), 036802.

(15) Chi, Z.; Yen, F.; Peng, F.; Zhu, J.; Zhang, Y.; Chen, X.; Yang, Z.; Liu, X.; Ma, Y.; Zhao, Y.; et al. Ultrahigh pressure superconductivity in molybdenum disulfide. arXiv:1503.05331, 2015.

(16) Nayak, A. P.; Yuan, Z.; Cao, B. X.; Liu, J.; Wu, J. J.; Moran, S. T.; Li, T. S.; Akinwande, D.; Jin, C. Q.; Lin, J. F. Pressure-modulated conductivity, carrier density, and mobility of multi layered tungsten disulfide. *ACS Nano* **2015**, *9* (9), 9117−9123.

(17) Han, Y. H.; Gao, C. X.; Ma, Y. Z.; Liu, H. W.; Pan, Y. W.; Luo, J. F.; Li, M.; He, C. Y.; Huang, X. W.; Zou, G. T. Integrated microcircuit on a diamond anvil for high-pressure electrical resistivity measurement. *Appl. Phys. Lett.* **2005**, *86* (6), 064104.

(18) Hu, T. J.; Cui, X. Y.; Gao, Y.; Han, Y. H.; Liu, C. L.; Liu, B.; Liu, H. W.; Ma, Y. Z.; Gao, C. X. *In situ* Hall effect measurement on diamond anvil cell under high pressure. *Rev. Sci. Instrum.* **2010**, *81* (11), 115101−115104.

(19) Rotundu, C. R.; Cuk, T.; Greene, R. L.; Shen, Z. X.; Hemley, R. J.; Struzhkin, V. V. High-pressure resistivity technique for quasi-hydrostatic compression experiments. *Rev. Sci. Instrum.* **2013**, *84* (6), 063903−063906.

(20) Funamori, N.; Sato, T. A cubic boron nitride gasket for diamond-anvil experiments. *Rev. Sci. Instrum.* **2008**, *79* (5), 053903−053908.

(21) Li, H.; Zhang, Q.; Yap, C. C. R.; Tay, B. K.; Edwin, T. H. T.; Olivier, A.; Baillargeat, D. From bulk to monolayer MoS_2: Evolution of Raman scattering. *Adv. Funct. Mater.* **2012**, *22* (7), 1385−1390.

(22) Saha, S.; Muthu, D. V. S.; Golberg, D.; Tang, C.; Zhi, C.; Bando, Y.; Sood, A. K. Comparative high pressure Raman study of boron nitride nanotubes and hexagonal boron nitride. *Chem. Phys. Lett.* **2006**, *421* (1−3), 86−90.

(23) Radisavljevic, B.; Radenovic, A.; Brivio, J.; Giacometti, V.; Kis, A. Single-layer MoS_2 transistors. *Nat. Nanotechnol.* **2011**, *6* (3), 147−150.

(24) Pradhan, N. R.; Rhodes, D.; Xin, Y.; Memaran, S.; Bhaskaran, L.; Siddiq, M.; Hill, S.; Ajayan, P. M.; Balicas, L. Ambipolar molybdenum diselenide field-effect transistors: field-effect and Hall mobilities. *ACS Nano* **2014**, *8* (8), 7923−7929.

(25) Late, D. J.; Liu, B.; Matte, H. S. S. R.; Dravid, V. P.; Rao, C. N. R. Hysteresis in single-layer MoS_2 field effect transistors. *ACS Nano* **2012**, *6* (6), 5635−5641.

(26) Shi, G.; Hanlumyuang, Y.; Liu, Z.; Gong, Y. J.; Gao, W. L.; Li, B.; Kono, J.; Lou, J.; Vajtai, R.; Sharma, P.; et al. Boron nitride-graphene nanocapacitor and the origins of anomalous size-dependent increase of capacitance. *Nano Lett.* **2014**, *14* (4), 1739−1744.

(27) Solozhenko, V. L.; Will, G.; Elf, F. Isothermal compression of hexagonal graphite-like boron-nitride up to 12 GPa. *Solid State Commun.* **1995**, *96* (1), 1−3.

(28) Akamaru, F.; Onodera, A.; Endo, T.; Mishima, O. Pressure dependence of the optical-absorption edge of AlN and graphite-type BN. *J. Phys. Chem. Solids* **2002**, *63* (5), 887−894.

(29) Ravindra, N. M.; Ganapathy, P.; Choi, J. Energy gap-refractive index relations in semiconductors-An overview. *Infrared Phys. Technol.* **2007**, *50* (1), 21−29.

(30) Das, S.; Chen, H. Y.; Penumatcha, A. V.; Appenzeller, J. High performance multilayer MoS_2 transistors with scandium contacts. *Nano Lett.* **2013**, *13* (1), 100−105.

(31) Dou, X. M.; Ding, K.; Jiang, D. S.; Fan, X. F.; Sun, B. Q. Probing spin-orbit coupling and interlayer coupling in atomically thin molybdenum disulfide using hydrostatic pressure. *ACS Nano* **2016**, *10* (1), 1619−1624.

(32) Guo, H. H.; Yang, T.; Tao, P.; Wang, Y.; Zhang, Z. D. High pressure effect on structure, electronic structure, and thermoelectric properties of MoS_2. *J. Appl. Phys.* **2013**, *113* (1), 013709−013715.

(33) Yokogawa, K.; Murata, K.; Yoshino, H.; Aoyama, S. Solid-ification of high-pressure medium Daphne 7373. *Jpn. J. Appl. Phys. 1* **2007**, *46* (6A), 3636−3639.

(34) Chijioke, A. D.; Nellis, W. J.; Soldatov, A.; Silvera, I. F. The ruby pressure standard to 150 GPa. *J. Appl. Phys.* **2005**, *98* (11), 114905−114913.